Super-resolution with a positive epsilon multi-quantum-well super-lens

A. O. Bak, V. Giannini, S. A. Maier, and C. C. Phillips

Super-resolution with a positive epsilon multi-quantum-well super-lens

A. O. Bak, V. Giannini, S. A. Maier, and C. C. Phillips[a)]

Experimental Solid State Group, Department of Physics, Imperial College London, London SW7 2AZ, United Kingdom

We design an anisotropic and dichroic quantum metamaterial that is able to achieve super-resolution without the need for a negative permittivity. When exploring the parameters of the structure, we take into account the limits of semiconductor fabrication technology based on quantum well stacks. By heavily doping the structure with free electrons, we infer an anisotropic effective medium with a prolate ellipsoid dispersion curve which allows for near-diffractionless propagation of light (similar to an epsilon-near-zero hyperbolic lens). This, coupled with low absorption, allows us to resolve images at the sub-wavelength scale at distances 6 times greater than equivalent natural materials. © 2013 AIP Publishing LLC. [http://dx.doi.org/10.1063/1.4859715]

In 1968, Veselago[1] predicted counter intuitive behavior in negative index materials where the permittivity, ϵ, and permeability, μ, are both negative. In 2000, Pendry[2] suggested a perfect lens to achieve super-resolution in the electrostatic limit, with materials exhibiting only $\epsilon < 0$. Since then metamaterials have been devised that are able to achieve super-resolution in the near-field, operating from microwave through to optical wavelengths.[3–6] Salandrino and Engheta[7] suggested an anisotropic metamaterial which is able to support near-diffractionless propagation of light: an epsilon-near-zero (ENZ) hyperlens which, when used in a cylindrical geometry, is able to super-resolve in the far-field.[8,9]

Such metallic metamaterials usually suffer from high losses due to high absorption where $\epsilon < 0$. This is a natural consequence of causality; however, some attempts have been made to decouple absorption from the region of interest by employing non-metallic anisotropic metamaterials.[10] Here, by utilizing extreme anisotropy to achieve near-diffractionless propagation of light, we present a metamaterial design which is able to achieve super-resolution at distances comparable to the effective wavelength of incident light, in the infrared (IR) part of the spectrum. This is a similar concept to the ENZ hyperlens but with an important difference: our super-resolution regime occurs in the spectral region where $\epsilon > 0$ which gives lower absorption loss. We are able to achieve super-resolution at distances comparable to the effective wavelength of incident light with a simple planar geometry.

We propose a periodically layered doped-GaAs/Al$_{0.3}$Ga$_{0.7}$As semiconductor structure, as shown in Fig. 1(a), where the layers are thin enough to quantize the electron energy levels in the direction of periodicity. The structure therefore behaves as a Multi-Quantum-Well (MQW), with the GaAs and Al$_{0.3}$Ga$_{0.7}$As layers being the well and barrier, respectively, as described in Fig. 1(b). Atomic-like *intersubband transitions* (ISBTs) are possible between the ground, $|1\rangle$, and the excited, $|2\rangle$, electron energy states within the QW.

Layered semiconductors have previously been shown to offer remarkable propagation and imaging characteristics by structuring the geometry on a sub-wavelength scale and modifying the metamaterial response according to classical electromagnetic theory.[7,10] However, our structures also modify the dielectric responses of the component materials themselves, as the layers are now thin enough to modify, via quantum theory, the allowed electron transitions within
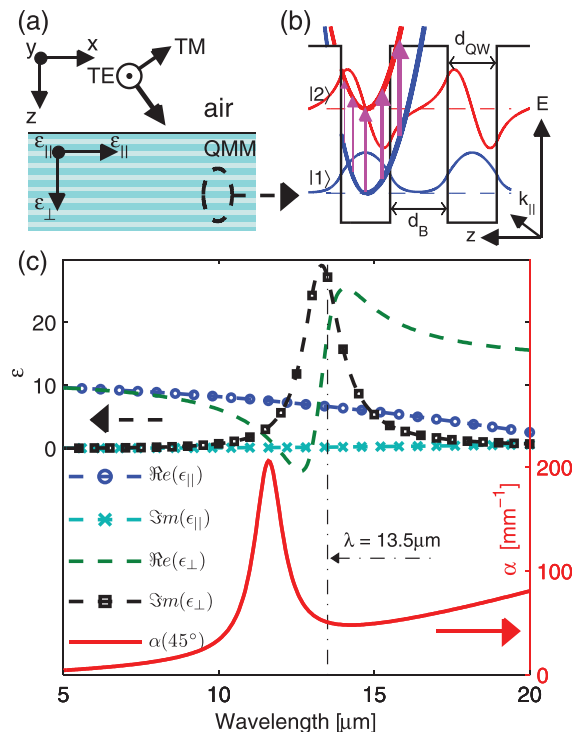

FIG. 1. (a) The QMM design: GaAs and Al$_{0.3}$Ga$_{0.7}$As layers are periodically repeated in the z direction. The QMM is anisotropic with $\epsilon_\perp$ in the z-direction and $\epsilon_\parallel$ in the x- and y-direction. (b) Illustration of electron energy confinement in the quantum wells where d_B is the barrier width, d_{QW} is the well width, $|1\rangle$ and $|2\rangle$ are the ground and excited energy states, respectively. The dispersion relation of Q2DEG, illustrated in the left quantum well, forms the subbands of the ground and excited states; the arrows represent the ISBT between the two subbands. (c) The dotted lines represent the real and imaginary components of $\epsilon_\parallel$ and $\epsilon_\perp$. The solid line is the absorption coefficient, α, peaking at the ISBT energy.

[a)]Electronic mail: chris.phillips@imperial.ac.uk

103, 261110-1

them. They are termed quantum metamaterials[11] (QMM) to denote the extra design flexibility this brings.

The AlGaAs barriers are wide enough to inhibit tunneling between the GaAs wells. Although the electrons in adjacent wells are coupled to each other electrostatically, they are not coupled quantum mechanically. The electrons are therefore confined to move only in the planes of the GaAs wells and form a quasi-2-dimensional-electron-gas (Q2DEG) with a Drude response to electric fields polarized in the plane of the wells.[12] As the electrons occupy a continuum of momentum states within this plane, each of the two quantized energy states forms a *subband* with a parabolic dispersion relation, as shown in Fig. 1(b). However, because both dispersion relations are parallel to each other the ISBT energy is equal for all electron momenta and, for electric fields polarized in the direction perpendicular to the wells, electrons undergo a transition with zero in-plane momentum change. This leads to a sharp Lorentzian-like ISBT line homogeneously broadened only by the natural lifetime of each state.

The QW width controls the peak energy of the ISBT. To maximise the elliptical nature of the isofrequency dispersion curve, we need the strongest and sharpest possible ISBT absorption peak, corresponding to the largest practical doping level. To be practical, a limit on the doping level needs to be considered: (a) the maximum amount, $\approx 4 \times 10^{18} \, \text{cm}^{-3}$, achievable with available semiconductor fabrication techniques, (b) such that the Fermi energy is below $|2\rangle$, the first excited energy state. If the doping density is too high and the Fermi energy is above $|2\rangle$, then the strength of the $|1\rangle$ to $|2\rangle$ ISBT will be reduced.

The individual semiconductor layers are very much subwavelength in thickness and the MQW structure can be described, to a good approximation, as an effective anisotropic dielectric medium. This is discussed in detail in Ref. 13, and we use that method, with the following parameters, to calculate the effective dielectric response of the QMM (plotted in Fig. 1(c)): background dielectric constants of $\epsilon_{\infty GaAs} = 10.64$ and $\epsilon_{\infty Al0.3Ga0.7As} = 9.92$; a GaAs QW width, $d_{QW} = 8.5 \, \text{nm}$ with a doping density of $3.1 \times 10^{18} \, \text{cm}^{-3}$ such that the Fermi energy is 90% of the ISBT energy; an $Al_{0.3}Ga_{0.7}As$ barrier width, $d_B = 10 \, \text{nm}$; a linewidth that is 10% of the ISBT energy at full-width-half-maximum (FWHM). The narrower the linewidth the stronger the ISBT transition, which is preferable when aiming to achieve high eccentricity in the isofrequency dispersion curves. Here, we use a demanding but realistic linewidth of 10 meV at FWHM. The ISBT energy itself and the oscillator strength are calculated using a finite difference tri-diagonal matrix method.[14]

For isotropic media, the Kramers-Kronig relationship between the real and imaginary parts of a complex function implies that a sizable modulation in the real part of the permittivity is usually accompanied by relatively high absorption, as, with the isotropic case, the imaginary part of the permittivity is directly proportional to the absorption. However, for an anisotropic medium, the peak of the imaginary part of $\epsilon_\perp$ is shifted away from the ISBT energy (see Fig. 1(c)). This means that material properties such as negative $\epsilon_\perp$ and high positive $\epsilon_\perp$, which determine the

super-resolution behaviour of our material, will be accompanied by lower absorption than would be seen in traditional isotropic metamaterials. The region with $\epsilon_\perp < 0$ has been discussed previously in Ref. 15, here we consider super-resolution imaging within the high $\epsilon_\perp$ region.

There is a further reduction in absorption within the high $\epsilon_\perp$ spectral region due to the quantization effect. For a non-quantized anisotropic medium, for example, in Ref. 10, the effective permittivity in all directions is governed by the underlying Drude response of one of the media. In that case, of the two zero crossings in $\Re e(\epsilon_\perp(\lambda))$, the longer wavelength one coincides with the zero crossing in $\Re e(\epsilon_\parallel(\lambda))$. However, in our case, the QMM is governed by two different physical mechanisms: the Q2DEG in the parallel direction follows the Drude absorption model, whilst in the perpendicular direction the ISBT absorption is governed by quantum mechanics. Therefore, as seen in Fig. 1(c), the longer wavelength zero crossing of $\Re e(\epsilon_\perp)$ is shifted from the wavelength when $\Re e(\epsilon_\parallel) = 0$. This separates the two types of absorption spectra, in particular, the Drude absorption part is red-shifted to longer wavelengths with respect to the ISBT, thereby reducing the overall sample absorption in the high $\epsilon_\perp$ spectral region.

As well as being anisotropic, the QMM shows extreme dichroism—such that only the transverse magnetic (TM) polarisation of light, the one where the magnetic field is parallel to the plane of interface, is affected by the absorption due to the ISBT. We model the propagation of light through the QMM with the analytical transfer matrix method[16] and show the absorption profile for a TM wave at 45° incidence in Fig. 1(c). It can be seen that the Lorentzian peak of the ISBT is superposed on the Drude absorption from the Q2DEG. Due to the anisotropy, the xy-component of the electric field of the traveling wave interacts with the Drude absorption of the Q2DEG, while the z-component interacts with absorption from the ISBT.

When propagating through the QMM, due to the anisotropy, an incident TM wave will experience a combination of both the perpendicular, $\epsilon_\perp$, and parallel, $\epsilon_\parallel$, dielectric responses; the relative contribution of each component will be angle dependent. To demonstrate super-resolution qualities we shall focus on the spectral region where $\epsilon_\perp$ goes through a maximum, $\lambda \approx 13.5 \, \mu\text{m}$. Around this maximum, the isofrequency dispersion curves, depicted in Fig. 2(a), form a prolate ellipsoid. As $\epsilon_\perp > \epsilon_\parallel$ by almost one order of magnitude, the ellipsoid is heavily stretched, and as seen in Fig. 2(a), wavevectors from all incident angles are transmitted onto an almost flat part of the elliptical dispersion curve. The Poynting vector is perpendicular to the gradient of the dispersion ellipse, and therefore the transmitted energy flow for all incident angles is almost parallel within the QMM, giving near-diffractionless propagation of light. Salandrino and Engheta[7] use a similar argument to show near-diffractionless propagation of light for an ENZ anisotropic metamaterial with flat hyperbolic dispersion curves.

The overall absorption experienced within the QMM is, nevertheless, dependent on the incident angle, θ_i, since the material is inherently anisotropic and the orientation of the electric field vector determines the relative amount of ISBT and Drude absorption the light experiences. The Figure of
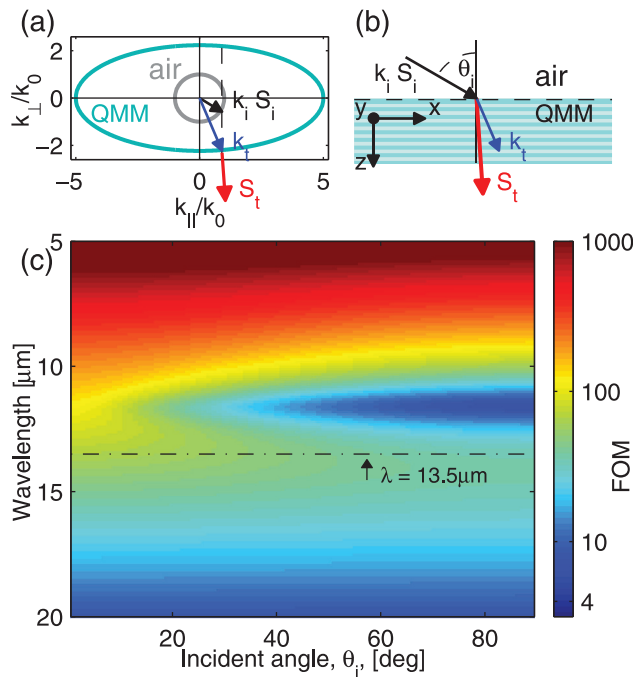
FIG. 2. (a) The isofrequency dispersion curves for the QMM and air at $\lambda = 13.5\,\mu m$. All incident wavevectors in air, k_i, are transmitted into the QMM as k_t and fall onto a flat part of the dispersion curve since the dielectric constant in air is much smaller than that of the QMM. The Poynting vector, S_t, shows the direction of energy flow within the QMM and is defined as being perpendicular to the gradient of the dispersion ellipse at k_t. Over the range of k_t values corresponding to a full 180° spread in θ_i, the incident k_i angles, the direction of S_t varies by less than 11° about the sample normal. (b) The same vectors as in (a) are depicted in real space; θ_i defines the incident angle. Plotted in (c) is the Figure of Merit for a TM wave, $FOM = \Re e(k_{TM})/\Im m(k_{TM})$, for all incident angles at varying wavelengths. As the QMM is anisotropic, the optical properties depend on the angle of incidence: for zero angle of incidence, no absorption from ISBT can be seen, and as the incident angle increases, the absorption from the ISBT increases.

Merit for a TM wave, $FOM = \Re e(k_{TM})/\Im m(k_{TM})$, which is inversely related to the absorption, is shown in Fig. 2(c) for all incident angles within the mid-IR spectrum.

Within the wavelength range of $13\,\mu m$ to $15\,\mu m$, where the $\epsilon_\perp$ goes through a maximum, which coincides with the local absorption minima (see Fig. 1(c)), the FOM ranges from 30 (for $\theta_i = 90°$) to 75 (for $\theta = 0°$). This is approximately one order of magnitude larger than those reported from non-quantized anisotropic metamaterials.[10] In particular, at $13.5\,\mu m$, the number of effective wavelengths in the QMM within an absorption depth of $1/\alpha$, where α is the absorption coefficient for the TM wave, is calculated to range from 4.7 at 90° incidence to 9.0 for 0° incidence.

This low absorption, matched with a high anisotropy between $\epsilon_\perp$ and $\epsilon_\parallel$, presents an opportunity for near-diffractionless propagation of light over comparatively large distances. To demonstrate this, we simulate the propagation of light passing through a mask of sub-wavelength dimensions into the QMM by means of solving Maxwell's equations in 3-dimensions with the finite-difference-time-domain (FDTD) method, using the commercial programme Lumerical.

The system studied is illustrated in Fig. 3(a), where two circular holes are etched-out of a 300 nm thick gold layer, with a diameter of $1.4\,\mu m$ each and an edge-to-edge separation of 600 nm. They are illuminated from above with mid-
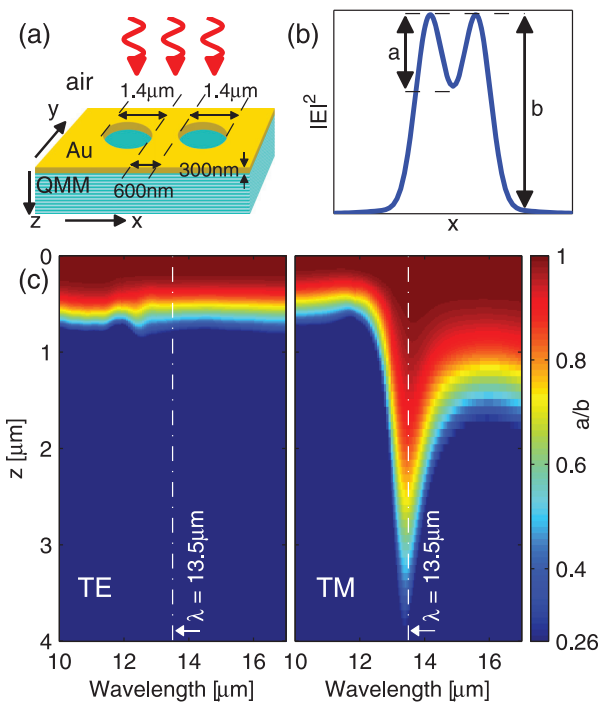

FIG. 3. (a) The geometric set-up used in the simulation. (b) Illustration defining the resolution: the electric field intensity profile, $|E(x)|^2$, along x is taken at $y = 0$ (i.e., at the center of the circular holes when looking in the y-direction); the ratio between the peak to trough height, a, and the peak height, b, define the resolution as a/b. (c) The resolution, as defined by (b), for a range of wavelengths, $10\,\mu m < \lambda < 17\,\mu m$, and at increasing distances, z, from the gold mask—for both TM and TE incident waves. For the TM waves, at $13.5\,\mu m$, the image is resolved up to a distance of $z = 4\,\mu m$ away from the mask. The resolution for the TE wave is shown for comparison.

IR radiation with wavelengths ranging from $10\,\mu m$ to $17\,\mu m$. The gold mask sits between air and the QMM.

The resolution is defined as the contrast ratio between the peak, b, and the trough, a, of the intensity profile on the zx-plane that intersects the centers of both circles and is illustrated in Fig. 3(b). According to the Rayleigh criterion, the spots are resolved when $a/b \geq 0.26$. The resolution ratio, a/b, is shown in Fig. 3(c) for varying wavelengths of illumination and at increasing distances away from the gold mask; values below the 0.26 Rayleigh limit are not mapped.

To emphasize, we are imaging two sub-wavelength circular holes with an edge-to-edge separation of 600 nm with wavelengths between $10\,\mu m < \lambda < 17\,\mu m$—this is very much below the natural diffraction limit. Of course, all materials are able to super-resolve in the very-near-field; however, the simulation shows that the proposed QMM is able to super-resolve at much larger distances.

The distance at which the image is super-resolved with the QMM is almost 6 times greater than can be achieved with bulk GaAs, one of the constituent materials in the QMM. Furthermore, we use a control simulation with a loss-less, isotropic material with $\epsilon = 25$ (equivalent to the maximum $\epsilon_\perp$ of the QMM) for comparison. As seen in Fig. 4, the QMM is able to super-resolve the image, while the isotropic material does not. This clarifies that the super-resolution effect is not only due to the high refractive index, but is indeed a consequence of the tailored optical response of the QMM itself. Using the control simulation, we calculate that the QMM resolves the image at distances at least 4 times
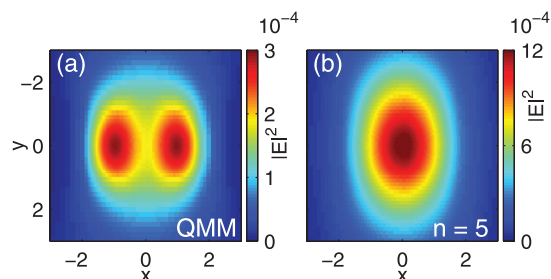
FIG. 4. A comparison of electric field intensity, $|E(x,y)|^2$, at $z = 3\,\mu m$ and $\lambda = 13.5\,\mu m$ between (a) the QMM and (b) a hypothetical lossless isotropic material with $\epsilon = 25$.

greater than any lossless, isotropic material with $\epsilon > 1$, as long as ϵ is such that the mask is considered to be sub-wavelength at the effective wavelength, i.e., $\lambda_{eff} = \lambda/\sqrt{\epsilon}$.

The maximum distance, $z_{max}(\lambda = 13.5\,\mu m)$, at which the sub-wavelength pattern can be resolved is approximately $4\,\mu m$ (see Fig. 3(c)). We see that the reduced overall absorption within the high $\epsilon_\perp$ spectral region has increased the ratio z_{max}/λ_{eff}, the maximum resolved distance in units of λ_{eff} to values that range between 0.77 (for $\theta_i = 0°$) and 1.20 ($\theta_i = 90°$). This means that with a planar geometry structure we are able to resolve sub-wavelength features at distances comparable to one effective wavelength.

We discuss a QMM design with low absorption and a positive ϵ which is able to propagate light in a near-diffractionless manner. Employing realistic design parameters, we show that sub-wavelength resolution can be achieved at distances 6 times greater than equivalent natural materials. The propagation of light experiences reduced absorption due to the quantization and anisotropy on account of the fact that the ISBT absorption peak is red-shifted away from the super-resolution spectral region. We find a maximum $FOM = 75$ for a QMM with realistic design parameters. Further potential could be realised by using these QMM in a cylindrical topology as suggested by Ref. 7, which would enable for super-resolution imaging further in the far-field.

[1]V. Veselago, Phys. Usp. **10**, 509 (1968).
[2]J. B. Pendry, Phys. Rev. Lett. **85**, 3966 (2000).
[3]N. Fang, H. Lee, C. Sun, and X. Zhang, Science **308**, 534 (2005).
[4]D. R. Smith, J. B. Pendry, and M. C. K. Wiltshire, Science **305**, 788 (2004).
[5]J. Valentine, S. Zhang, T. Zentgraf, E. Ulin-Avila, D. A. Genov, G. Bartal, and X. Zhang, Nat. Lett. **455**, 376 (2008).
[6]T. Taubner, D. Korobkin, Y. Urzhumov, G. Shvets, and R. Hillenbrand, Science **313**, 1595 (2006).
[7]A. Salandrino and N. Engheta, Phys. Rev. B **74**, 075103 (2006).
[8]J. Rho, Z. Ye, Y. Xiong, X. Yin, Z. Liu, H. Choi, G. Bartal, and X. Zhang, Nat. Commun. **1**, 143 (2010).
[9]S. Han, Y. Xiong, D. Genov, Z. Liu, G. Bartal, and X. Zhang, Nano Lett. **8**, 4243 (2008).
[10]A. J. Hoffman, L. Alekseyev, S. S. Howard, K. J. Franz, D. Wasserman, V. A. Podolskiy, E. E. Narimanov, D. L. Sivco, and C. Gmachl, Nature Mater. **6**, 946 (2007).
[11]J. R. Plumridge, R. J. Steed, and C. C. Phillips, Phys. Rev. B **77**, 205428 (2008).
[12]J. R. Plumridge and C. C. Phillips, Phys. Rev. B **76**, 075326 (2007).
[13]M. Zaluzny and C. Nalewajko, Phys. Rev. B **59**, 13043 (1999).
[14]T. Horikis, Phys. Lett. A **359**, 345 (2006).
[15]K. Yang, V. Giannini, A. O. Bak, H. Amrania, S. A. Maier, and C. C. Phillips, Phys. Rev. B **86**, 075309 (2012).
[16]P. Yeh, *Optical Waves in Layered Media*, 2nd ed. (Wiley, 2005).